# Reexamining $CO_2$ Storage Capacity and Utilization of the Utsira Formation

Odd Andersen* (SINTEF) Halvor Møll Nilsen (SINTEF)
Knut-Andreas Lie (SINTEF)

July 1, 2014

**Abstract**

In this work we provide estimates of $CO_2$ storage capacity of the Utsira Formation using the recently provided datasets from the Norwegian Petroleum Directorate, taking $CO_2$ density variation into account. We also investigate strategies on how to realize as much as possible of this potential in large-scale injection scenarios. We base our study on the assumption that the limiting factor for $CO_2$ storage at Utsira is the efficient use of available trapping mechanisms, with pressure buildup being of secondary concern. We consider the trapping mechanisms considered most important for the medium-to-long term (structural, residual and dissolution trapping), using a combination of modeling tools based on the Matlab Reservoir Simulation Toolbox (MRST).

## Introduction

The Utsira Formation is a large saline aquifer covering some 26.000 square kilometers (Chadwick et al., 2012), consisting of a more than a hundred meter thick column of high-permeability sand. The formation has been used as a target for industrial-scale $CO_2$ sequestration since 1996, where the injected $CO_2$ is a by-product from natural gas extraction at the nearby Sleipner Vest field (Baklid et al., 1996). Since then, approximately 1 Mt of $CO_2$ has been injected per year. While this storage operation is unique in its kind, the involved quantity falls far short of the storage potential of the site, and remains insignificant compared to the quantities necessary for CCS to be a significant part of an European greenhouse gas mitigation scenario. For instance, net European $CO_2$ emissions from energy industries, manufacturing and construction (comprising the industries for which CCS can be considered at least nominally possible) totaled 1.95 Gt in 2011 (UNFCCC, 2011). If CCS with geological storage were to handle a significant amount of this, hundreds of megatonnes of $CO_2$ would need to be injected annually into geological formations for permanent storage, orders of magnitude above current operations at Utsira.

Several capacity figures for the Utsira aquifer have been published in previous literature. A summary table in (Thibeau and Mucha, 2011) provides an overview, where estimated total capacity ranges from 0.3 Gt (Chadwick et al., 2008) to 20–60 Gt (Lindeberg et al., 2009). The large variation in published estimates is due to different assumptions made, in particular to what is considered the main limiting factors. If the aquifer is considered closed, or with low hydraulic connectivity, then pressure buildup becomes the main concern. The estimates in (Lindeberg et al., 2009; Thibeau and Mucha, 2011) are based on the prevention of excessive pressure buildup, and the 60 Gt estimated figure from (Lindeberg et al., 2009) is arrived at by assuming extensive production of formation water to alleviate pressure buildup from $CO_2$ injection into a closed system. On the other hand, if the aquifer is considered open with good hydraulic connectivity, leakage risk due to long-term $CO_2$ migration typically becomes the main limiting factor on storage capacity. In that case, the central issue defining storage capacity is the amount of $CO_2$ the storage site can retain over time by various trapping mechanisms. The most immediately available trapping mechanism is stratigraphic or structural trapping, where the $CO_2$ migration is blocked by low-permeability rock barriers. The lower figure of 0.3 Gt cited above only considers this type of trapping. Other available trapping mechanisms include residual trapping, dissolution and mineral trapping, whose full potential cannot be efficiently realized, or happen over much longer time spans.

In 2011, the Norwegian Petroleum Directorate released a $CO_2$ Storage Atlas of the North Sea (Halland et al., 2011), providing detailed models of twenty-one formations having the potential for $CO_2$ storage. In the $CO_2$ Storage Atlas, the Utsira Formation is classified as an open aquifer and the corresponding model includes caprock depth and thickness values over the full range of the aquifer in the Norwegian sector. The storage capacity of the combined Utsira–Skade system is estimated to be 16 Gt, with a prospectivity of 0.5–1.5 Gt. Pressure buildup at the site has been studied by Chadwick et al. (2012), who conclude that available pressure monitoring data suggests very minor pressure increases (perhaps 0.1 MPa) away from the injection point, consistent with little or no flow compartmentalization. Herein, we employ functionality from the $CO_2$-module of an open-source software (Lie et al., 2012; MRST) to reexamine the total storage capacity of the aquifer as described by the data set from the $CO_2$ Storage Atlas, and look at possible injection strategies for large-scale operations. While our study is simplistic in several aspects (e.g. assuming homogeneous rock properties and fully open boundaries), it sketches a possible approach for preliminary exploration of possible scenarios and estimation of realized trapping capacity.

## Method

In (Nilsen et al., 2014c) we describe how we generate an aquifer model of Utsira from the data provided in (Halland et al., 2011), using functionality available in the open-source Matlab Reservoir Simulation Toolbox (MRST). In addition to providing simple access to the $CO_2$ Storage Atlas data, the next release

of `MRST-co2lab` will include column-based storage estimates, geometrical analysis of the caprock (Nilsen et al., 2014c), vertical equilibrium simulators (Nilsen et al., 2014a,b), and optimization of well placement and injection rates (Lie et al., 2014).

*Data and assumptions*

In the present work, we use the atlas model of Utsira together with parameters from (Singh et al., 2010; Holloway et al., 2004; Chadwick et al., 2008), as listed in Table 11 to estimate volumetric trapping capacities. These parameters suggest a temperature at the depth of the current injection point of 40.2°C, in the middle of the suggested range of 36°C to 46°C from (Chadwick et al., 2008). We further use the equation-of-state for $CO_2$ specified by Span and Wagner (1996) to estimate local $CO_2$ densities and compute trapping capacity in terms of mass. By lack of more detailed data, rock porosity and residual saturations are assumed constant across the aquifer.

***Table 1*** *Parameter values used to estimate trapping capacities for the Utsira Formation.*

| Parameter | Value | Unit | Reference |
|---|---|---|---|
| Sea depth | 80 | m | Holloway et al. (2004) |
| Injection depth | 1012 | m | Singh et al. (2010) |
| Thermal gradient | 35.6 | °C/km | Singh et al. (2010) |
| Seabed temperature | 7 | °C | Singh et al. (2010) |
| Residual water saturation | 0.11 | | Singh et al. (2010) |
| Residual $CO_2$ saturation | 0.21 | | Singh et al. (2010) |
| Rock porosity | 0.36 | | Singh et al. (2010) |
| Water density | 1020 | kg/m$^3$ | Singh et al. (2010) |
| $CO_2$ solubility in brine | 53 | kg/m$^3$ | Chadwick et al. (2008) |

From the conclusions in (Chadwick et al., 2012) and the classification of the formation as an open aquifer (Halland et al., 2011), we base our capacity estimate on the assumption that the ability of the formation to ultimately retain injected $CO_2$ is the main limiting factor. We assume that any overpressure from the injection operation will dissipate over time, so that the long-term pressure regime is hydrostatic. We further assume long-term thermal equilibrium, with ambient temperature given by the thermal gradient and reference (seabed) temperature. Structural traps are identified and their volume assessed by geometric analysis of the caprock shape using the algorithms described in (Nilsen et al., 2014c). For dissolution trapping, the value for $CO_2$ solubility is taken from (Chadwick et al., 2008).

We consider the storage capacity of Utsira to be the maximum quantity of $CO_2$ that can be ultimately retained by structural, residual and dissolution trapping. Although the formation pore space can accommodate even larger quantities of $CO_2$, any amount in excess of this retaining capacity will migrate and ultimately escape the domain boundaries, potentially leaking back to the surface.

*Total trapping capacity of a vertical column*

If we approximate the formation geometry as a grid of vertical pillars, we can compute the trapping capacity of each such pillar separately, and add up to obtain the total capacity estimate. The height $H$ of a given pillar can be written $H = h_1 + h_2$, where $h_1 (\geq 0)$ represents the part contained within a structural trap, as illustrated in Figure 1.

For the part of the column that is within a structural trap, the full retaining capacity $Q_1$ is reached when the pore space is maximally saturated with $CO_2$ and the remaining brine contains the maximal amount of dissolved $CO_2$:

$$Q_1 = Ah_1\phi\left[s_{w,r}c_{max} + (1 - s_{w,r})\rho_{co_2}\right]. \tag{1}$$

Here, $A$ is the area of a lateral cross-section of the pillar, $\phi$ the rock porosity, $s_{w,r}$ the residual water

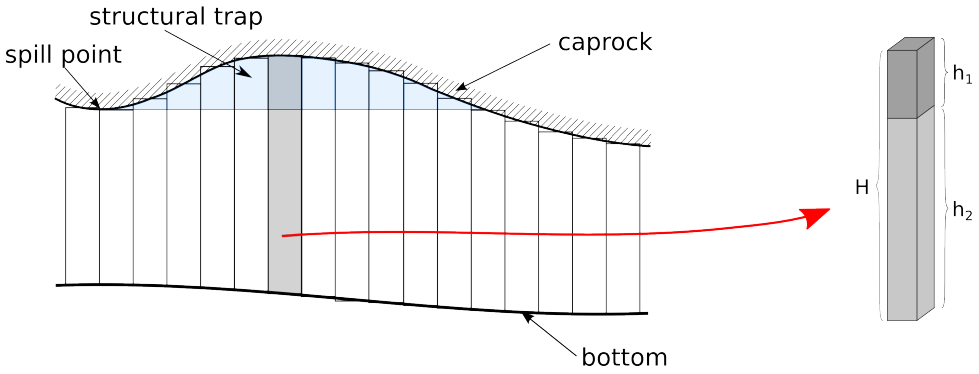


***Figure 1*** *Illustration of how the aquifer volume is divided into a mesh of pillars. Left: aquifer cross section. Right: a single pillar.*

saturation, $\rho_{co_2}$ the $CO_2$ density, and $c_{max}$ the maximum mass of $CO_2$ that can be dissolved per volume of formation water. We consider $\phi$ and $c_{max}$ to be constants as given in Table 1, whereas $\rho_{co_2}$ is a function of temperature and pressure.

Similarly, the part of the column not contained within a structural trap is at full retaining capacity $Q_2$ when all pore space contains the residual amount of $CO_2$ and all remaining brine contains the maximal amount of dissolved $CO_2$

$$Q_2 = Ah_2\phi\left[(1-s_{n,r})c_{max} + s_{n,r}\rho_{co_2}\right], \tag{2}$$

where $s_{n,r}$ represents the residual saturation of $CO_2$.

We now use superscript $i$ to denote a given pillar. The total retaining capacity of pillar $i$ is

$$Q^i = Q_1^i + Q_2^i \tag{3}$$

and the total estimate for the aquifer becomes

$$Q = \sum_i Q^i = \sum_i \left(D^i + S^i + R^i\right) = D + S + R, \tag{4}$$

where

$$\begin{aligned} D^i &= c_{max}\left[h_1^i s_{w,r} + h_2^i(1-s_{n,r})\right]A\phi, \\ S^i &= \rho_{co_2}^i\left[h_1^i(1-s_{w,r}) + h_2^i s_{n,r}\right]A\phi, \\ R^i &= \rho_{co_2}^i h_2^i s_{n,r} A\phi. \end{aligned}$$

Here, $D = \sum_i D^i$, $S = \sum_i S^i$, and $R = \sum_i R^i$ represent total $CO_2$ mass in the aquifer that can be retained by dissolution, structural trapping, and residual trapping, respectively.

**Potential storage capacity of the Utsira formation**

At the finest scale, our digital Utsira model is discretized using approximately one hundred thousand vertical pillars, each with a lateral cross-section of $500 \times 500$ m. Applying formula (3) on each pillar and summing up, we obtain the figures presented in Table 2. From this calculation, the estimated total trapping capacity of the aquifer surpasses 112 Gt, 69% of which is attributed to residual trapping. The aquifer has an estimated 1.13 Gt of structural trapping capacity, which is only 1% of the total figure.

Using values for the individual pillars, we construct a map of local storage capacity of the Utsira Formation (Figure 2, left). On this map, we note a wide range in local trapping capacities. Some pillars

***Table 2*** *Trapping capacity of the Utsira aquifer.*

| Type | Value [Gt] | % of total |
|---|---|---|
| Structural | 1.13 | 1.0 |
| Residual | 77.05 | 68.7 |
| Dissolution | 34.06 | 30.3 |
| Total | 112.24 | 100 |

are able to retain more than 4 Mt of $CO_2$ whereas others retain practically nothing. The highest local capacities are seen across a large region in the south. Another region with moderately high trapping capacities is located in the north. High storage capacities are associated with thick parts of the aquifer, particularly in the presence of structural traps and at depths where $CO_2$ is in a dense phase. A large part of the Utsira aquifer is so shallow that $CO_2$ will be in gas phase at equilibrium, resulting in significantly lower storage capacities. The boundary between regions with gas and liquid $CO_2$ can clearly be seen in the figure as a sharp, arch-shaped discontinuity that cuts into the aquifer from southwest and exits in the northwest.

For most open aquifers there will be no practical way of utilizing all, or even a significant fraction of the full storage capacity as defined above. Although the capacity of structural traps can in theory be fully exploited by strategic positioning of injection sites, efficient use of residual and dissolution trapping is hard to achieve. Because of density differences, $CO_2$ and brine will tend to separate after injection into separate volumes, with the $CO_2$ volume on top. The amount of residual trapping realized in a storage scenario will therefore depend on the sweep efficiency, i.e., the thickness of the migrating $CO_2$ plume compared to the local height of the aquifer. As the plume migrates and spreads out by buoyancy forces, it will also gradually thin out. Efficient use of residual trapping therefore mostly happens relatively close to the injection point, where the $CO_2$ plume still retains much of its initial thickness. Likewise, since dissolution of $CO_2$ into brine happens only gradually, dissolution trapping can improve the overall $CO_2$ retention rate at a given location only in the long-term presence of otherwise mobile $CO_2$.

In the middle diagram of Figure 2 we have plotted the combined capacity of pillars reachable by infinitesimal, purely gravity-driven migration originating from a given point in the model. We refer to this value as "total reachable capacity". In other words, if a small rate of $CO_2$ is continuously injected at some point in the aquifer, the reachable capacity value associated with that point is the total trapping capacity of all pillars encountered as the $CO_2$ migrates upwards following the steepest slope of the caprock. Whenever a structural trap is encountered, all pillars associated with that trap are considered reachable, since the $CO_2$ will accumulate there and spread out until the entire trap area is covered. The result is a plot with large, relative uniform regions associated with spill regions ("watersheds") connected with individual structural traps. This plot can be used as a simple heuristic to choose $CO_2$ injection locations associated with migration pathways that have high trapping potential. This should only be seen as an imperfect approach, in that it only considers infinitesimal flow, does not take sweep efficiency or migration speed (associated with caprock steepness) into account, and depends on the resolution of the aquifer model.

If we only consider structural trapping when computing reachable capacities, we end up with the right plot in Figure 2. We refer to the values thus obtained as representing "reachable structural capacity". The division of the aquifer into distinct regions is even stronger than for the middle figure, as any point associated with the spill region of a given trap has exactly the same value of reachable structural capacity. Although this plot disregards residual and dissolution trapping, it is more precise in what it covers, since structural capacity can in theory be fully utilized. When choosing an injection site with a goal of maximizing structural trapping only, "reachable structural capacity" thus provides clearer guidance than "total reachable capacity" does.

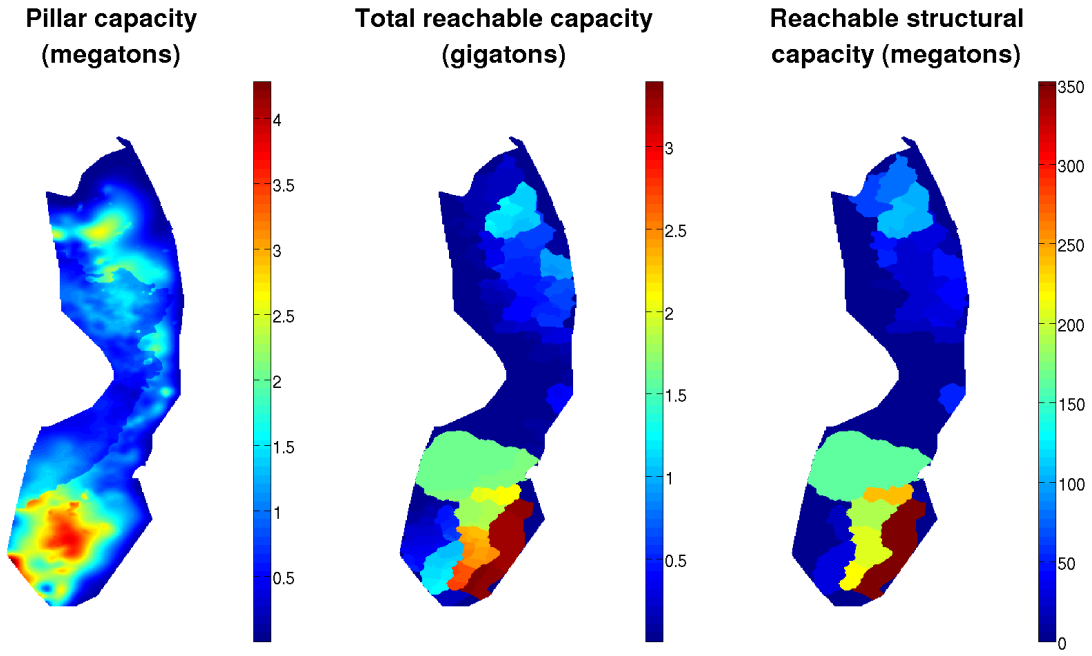


***Figure 2*** *Left: trapping capacity of individual vertical pillars in the Utsira model. Middle: combined trapping capacity reachable by gravity-driven migration from a given point. Right: combined structural trapping capacity reachable by gravity-driven migration from a given point.*

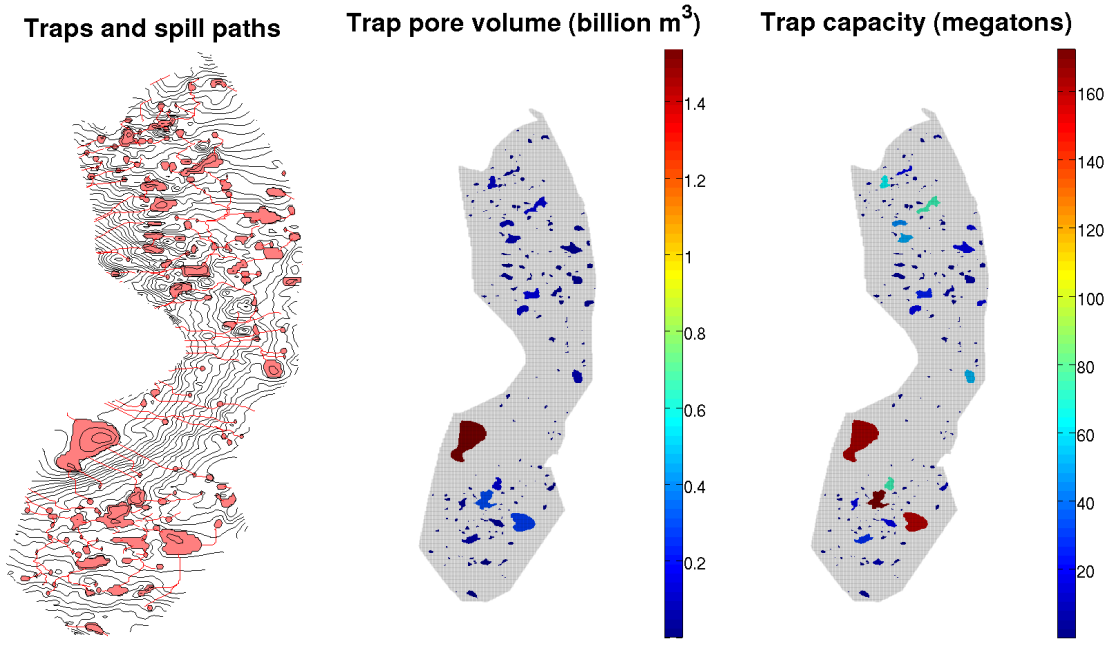


***Figure 3*** *Left: topographic map of the Utsira caprock, with structural traps and spill paths indicated. Middle: structural traps colored by pore volume. Right: structural traps colored by trapping capacity in mass terms.*

**Mapping the structural traps of Utsira**

Although structural traps only provide a very small fraction of the theoretical Utsira trapping capacity, they are important since they provide the most readily exploitable trapping mechanism, and because they slow down migration of the advancing $CO_2$ plume. A wide trap will make a narrow plume spread out, thus also facilitating dissolution.

In the left plot of Figure 3, we see a topographical map of the Utsira caprock with all traps and spill paths are traced out, as identified by a purely geometrical analysis. We observe an intricate, hierarchical system where multiple deeper traps spill into shallower ones along tributaries defined by spill paths. The largest traps are found in the southern parts of the aquifer. The general spill direction is from the east upwards into the shallower regions of the west.

In the middle plot of Figure 3, we have colored all the traps by total pore volume. We note that by this measure, the single largest trap by far is located in the southwest, with a pore volume of around 1.5 billion cubic meters. However, this does not translate directly into actual trapping capacity, presented in the rightmost plot of Figure 3. On this diagram, we see that the trap with the largest structural trapping capacity is now found in the middle of the southern region, where several other traps also gain prominence. The difference is due to varying $CO_2$ density. Indeed, the largest trap in terms of pore volume is located in a part of the aquifer where $CO_2$ is expected to be in gas phase, thus significantly reducing its structural trapping capacity.

**Injection strategies**

In practice, it will not be possible to exploit more than a small fraction of the total Utsira retaining capacity. However, our estimates serve as a theoretical upper bound on the quantity of $CO_2$ that can be stored at Utsira, and provide a reference for comparison when exploring possible injection scenarios. In the present section we identify and assess a few such scenarios. We choose injection locations and rates with the goal of maximizing the ultimately retained amount of $CO_2$. To do this, we employ a combination of spill-point analysis, "rapid" simulations and nonlinear optimization, all of which is functionality provided by MRST.

*Defining scenarios*

For our purposes, an injection scenario is defined by (1) the location of a given number of injection sites; and (2) the rates injected at each site over time. Our task is therefore to choose favorable injection sites and optimal injection schedules to maximize realized storage capacity and minimize leakages. In reality, there will naturally be logistical and other factors further constraining these choices, but we do not consider them here. However, such restrictions could be integrated in the proposed workflow by adding constraints and modifying the objective function of the optimization routine presented below.

Since structural traps provide the most immediately available and easiest to realize containment mechanism, a reasonable strategy would be to choose injection sites based on how much structural trapping capacity they can reach. To do this, we first map out the hierarchical system of structural traps, connecting spill paths and spill regions, and compute the storage capacity of each trap in mass terms. We can then apply a greedy algorithm to identify the set of injection point with the combined highest reachable structural capacity, adjusted to avoid double-counting (Lie et al., 2014). Since reachable structural capacity of all points within a given spill region is identical (cf. Figure 2, right), we use distance from model boundary as an additional selection criterion. In reality, flow will not be infinitesimal, so injecting $CO_2$ too close to the model boundary will often lead to significant leakage out of the domain even if the associated spill region leads into an internal trap.

Assuming that most of the injected $CO_2$ will migrate along the path predicted by caprock topography,

***Table 3*** *Simulation parameter values for optimization of injection rates*

| Parameter | Value | Unit | Reference |
|---|---|---|---|
| Injection period | 50 | year | |
| Migration period | 3000 | year | |
| $W$ (importance of leakage) | 10 | | |
| brine viscosity | $8 \cdot 10^{-4}$ | Pascal second | Singh et al. (2010) |
| $CO_2$ viscosity | $6 \cdot 10^{-5}$ | Pascal second | Singh et al. (2010) |
| rock permeability | 2 | Darcy | Singh et al. (2010) |

the reachable structural capacity figures provide immediate estimates on how much $CO_2$ can be injected at each site. Dividing these quantities by the total injection period results in relatively conservative injection rates compared to total expected trapping potential, since we expect additional trapping from capillarity and dissolution. The additional amount trapped by these mechanisms is hard to estimate a priori, but can be obtained from numerical simulation of the whole injection and migration phases. Vertical equilibrium (VE) modeling (Nilsen et al., 2014a) provides us with a tool to carry out simplified long-term simulations rapidly while respecting the most relevant physics. The ability to run multiple rapid simulations enables us to compute optimal injection schedules using nonlinear optimization. In this approach, the (fixed or time-dependent) injection rates at each site represent the variables of the problem, and we define an objective function that we seek to optimize. We here choose the objective function to be the combined total amount of $CO_2$ injected at all sites, minus the total amount of $CO_2$ escaped by the end of the simulation period multiplied by some weighting factor $W$. The use of this weighting factor enables us to specify the relative importance to be given to leakage compared to total amount injected – a high value of $W$ means little leakage is tolerated, and optimal injection rates will end up being lower. We solve the resulting optimization problem using a steepest descent method with gradients obtained by an adjoint method (Raynaud et al., 2014; Jansen, 2011) in combination with automatic differentiation. We optimize for scenarios in which the initial injection period is 50 years followed by a migration period of 3000 years. The weighting factor $W$ and other relevant simulation parameters used are listed in Table 3 (with the exception of those already listed in Table 1).

Even though the selection of injection sites is based solely on the maximization of structural trapping, the subsequent optimization of injection schedules allows us to take other trapping mechanisms into account. In principle, these would include at least residual and dissolution trapping. In the following examples however, we consider only structural and residual trapping for optimization of schedules, i.e., we disregard dissolution. There are two reasons for this. Firstly, including dissolution in VE simulations incur significant computational cost that would lead to very long runtimes for the optimization algorithm. This problem could partly be tackled by more fine-tuned algorithmic design, possibly on parallel hardware, but is a topic for future work. Secondly, while figures for $CO_2$ solubility in brine can be derived for Utsira conditions (cf. Table 1), little information exist on the effective dissolution *rates*. Theoretical studies indicate that if and when convective mixing between $CO_2$-saturated and unsaturated brine occurs, the subsequent dissolution rate will remain relatively constant until dissolution ends (Nordbotten and Celia, 2012). As the Utsira aquifer has a very high permeability, it is possible that significant convective mixing will happen. On the other hand, rate and onset time will likely be highly sensitive to the presence and vertical permeability of intra-reservoir mudstone barriers, which are observed at the Sleipner injection site. In the one-well example presented below, we carry out an additional simulation that includes dissolution trapping to show the potential impact. For simulation with dissolution, we use a rate of 0.44 kg per square meter per year. This is similar to the value used in (Gasda et al., 2011), which was there chosen by reference to theoretical studies. The impact of dissolution shown in the first example below should therefore be only understood as a qualitative illustration.

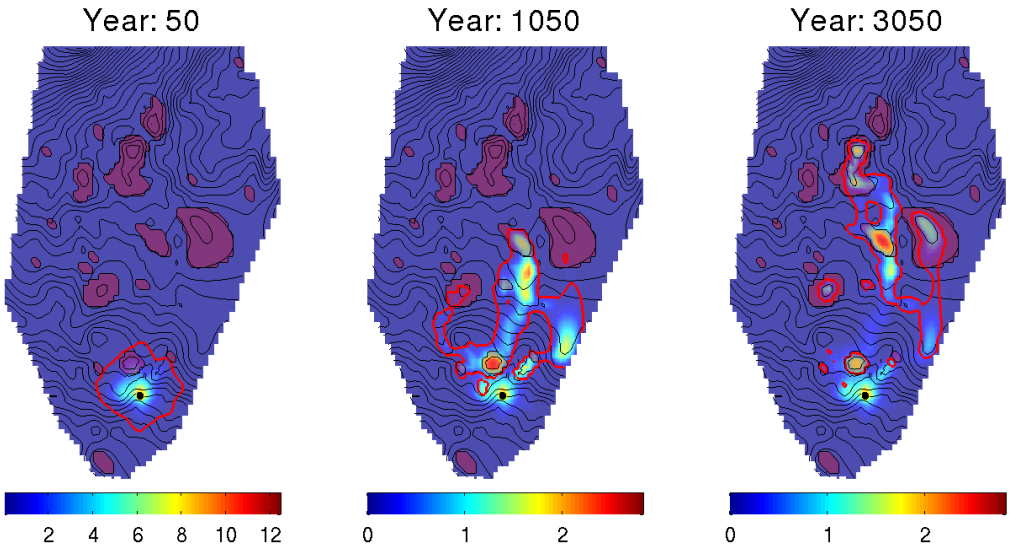


***Figure 4*** *Simulation of Scenario 1 with unoptimized injection rate. $CO_2$ plume outlined in red, structural traps overlaid in purple. Total vertical integrated $CO_2$ content indicated with color (unit: tonnes per lateral square meter).*

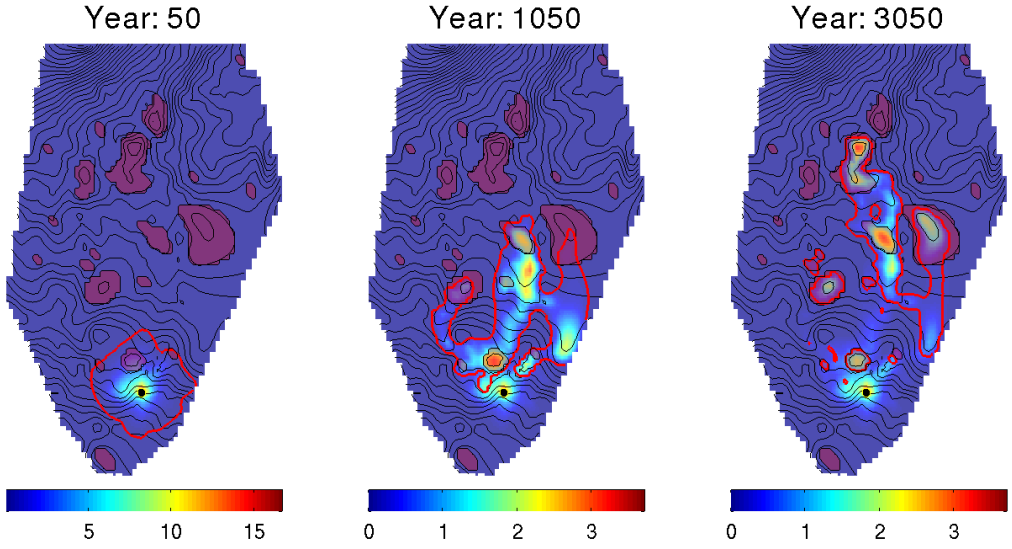


***Figure 5*** *Simulation of Scenario 1 after optimization of injection rate. $CO_2$ plume outlined in red, structural traps overlaid in purple. Total vertical integrated $CO_2$ content indicated with color (unit: tonnes per lateral square meter).*

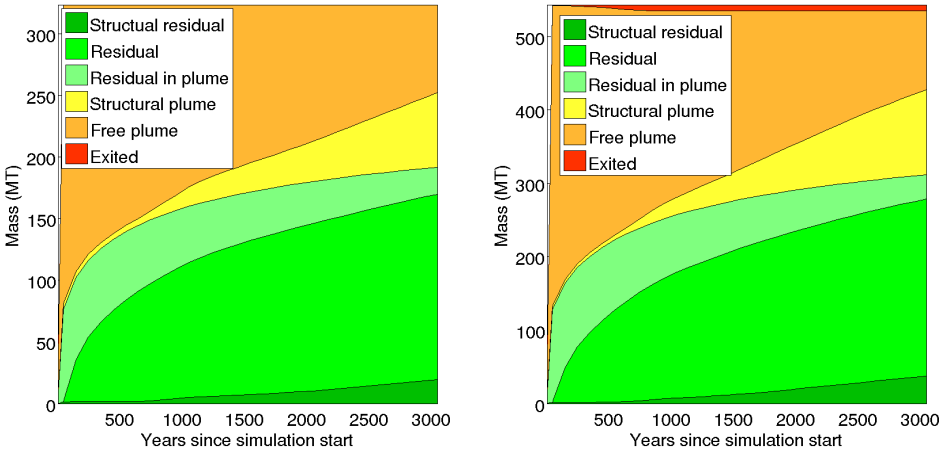


***Figure 6*** *Distribution of injected $CO_2$ in Scenario 1 as a function of time. Left diagram represents injection with unoptimized rates and right diagram with optimized rates.*

*Scenario 1: Injection from a single site*

In this example, we seek a good single-site injection scenario. Using reachable structural capacity as site selection criterion, we identify a location at the very south of the aquifer, indicated by a black dot in Figure 4 (only the part of the aquifer relevant for the subsequent simulation is shown). The reachable structural capacity at this point is 323 Mt, which translates into an injection rate (before optimization) of 6.46 Mt per year for 50 years. The outcome of a VE simulation of this scenario is presented in Figure 4, where the evolution of the $CO_2$ plume during the migration phase can be clearly seen. The moving plume leaves behind a trail of residually trapped $CO_2$. This is clearly visible on the color plot, which indicates total $CO_2$ content per square meter. We see that after 3000 years of migration, part of the $CO_2$ plume is located within structural traps but some is still migrating. This can also be seen in the left diagram of Figure 6, which shows the time-dependent distribution of injected $CO_2$ among various states of trapping, flow and leakage. We see that after 3000 years, free-flowing $CO_2$ outside traps ("Free plume") still represents a significant fraction of the injected quantity. The amount of $CO_2$ that has reached structural traps is indicated by "structural plume" and "structural residual", together making up approximately 25% of the total. Since the total amount injected equals the estimated reachable structural capacity, it is clear that most of this capacity has not been reached. This is partly due to the fact that migration has not yet ended, but another important factor is the large quantity of $CO_2$ that has become structurally trapped along the way ("Residual" and "Residual in plume"). It is clear from the figure that choosing an injection rate only based on reachable structural trapping can seriously underestimate actual realizable trapping capacity.

We now compute an optimal injection schedule as previously described. The outcome suggests a total amount of 543 Mt, injected at an almost-constant rate over the 50 year timespan. This is approximately 68% higher than for the unoptimized schedule. We re-run our scenario with this optimized schedule. The resulting migration is illustrated in Figure 5. We observe that the plume is now somewhat thicker, but has not migrated any further than in the previous case. However, more of the $CO_2$ has reached the trap at the northernmost tip of the plume, as can be read from the color plot. The right diagram in Figure 6 presents the corresponding $CO_2$ trapping distribution plot. We see that although the total quantity injected is significantly higher than for the unoptimized case, the relative share of each trapping mechanism remains roughly the same. In addition, we can see a thin red sliver at the top, which represents $CO_2$ that has escaped the domain (e.g., leaked). We note that the leakage happened during a period of some 800 years starting shortly after injection stop. From the previous plume plot (Figure 5) it is clear that this leakage occurred as the migrating plume brushed against the eastern border. The total amount escaped through the vertical boundaries is 8.5 Mt or 1.57% of the total injected quantity.

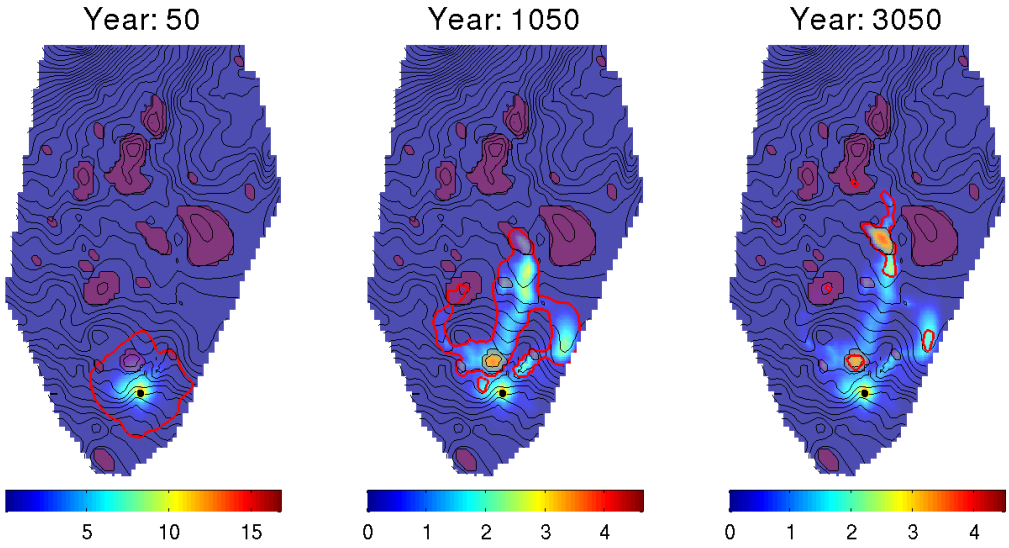


***Figure 7*** *Simulation of Scenario 1 after optimization of injection rate and with dissolution trapping included. $CO_2$ plume outlined in red, structural traps overlaid in purple. Total vertical integrated $CO_2$ content indicated with color (unit: tonnes per lateral square meter).*

To assess the potential impact of dissolution, we re-run the scenario with dissolution trapping enabled. We first do this for the optimized injection rates from the previous simulation. The resulting plume evolution is presented in Figure 7, where we note a dramatic difference from the case without dissolution. After 3000 years, only a few small isolated pockets of the $CO_2$ plume remain, and some traps have not been reached at all. From Figure 8, we see that most of the $CO_2$ has indeed dissolved in the brine. The total leakage has also been reduced to 0.7 Mt, or 0.13% of the total, which is too small to be visible on the figure.

We run the scenario once again, this time increasing the injection rate by 50%, for a total of 815 Mt over 50 years. The outcome is presented in Figure 9 and the right diagram of Figure 8. We see that while the plume reaches a bit farther this time, most of the $CO_2$ still ends up dissolved, and the amount that escapes across the vertical boundaries (7.8 Mt, or 0.96% of the total) is still lower than the original case without dissolution. This experiment suggests that by ignoring dissolution trapping, we run the risk of severely underestimating the amount of $CO_2$ that can will be trapped for a given scenario. Case-specific knowledge on dissolution rates at Utsira thus remains an important unknown in any attempt to predict long-term plume migration and realized storage capacity.

*Scenario 2: Injection from multiple sites*

By using multiple injection sites, a larger part of the aquifer can be reached. In this example, we define a scenario with ten sites. Site locations and injection schedules are chosen using the same approach as the previous example. The chosen sites can be seen as black dots on the plots in Figure 10. In addition to the injection site from the previous example, three more sites have been added to the southern region. The northern region is covered with five injection sites, whereas one injection site has been included in the narrow corridor connecting the two regions. This connecting corridor is relatively thin, steeply inclined, shallow, and contains few structural traps. It is thus of limited use for $CO_2$ storage, but the presence of a small trap to the northeast of the injection site led to the placement of the middle injection site.

Figure 10 shows the result of simulating the scenario before optimization of schedules. The total injected amount over the 50 year injection period is 894 Mt. As we can see on the corresponding distribution plot (Figure 11, left), this time almost 50% of the injected $CO_2$ reaches the structural traps during the simulation period. Another 40% ends up residually trapped, while approximately 10% either remains in the free part of the plume, or has escaped (1.45%, or 13 Mt, for the latter).

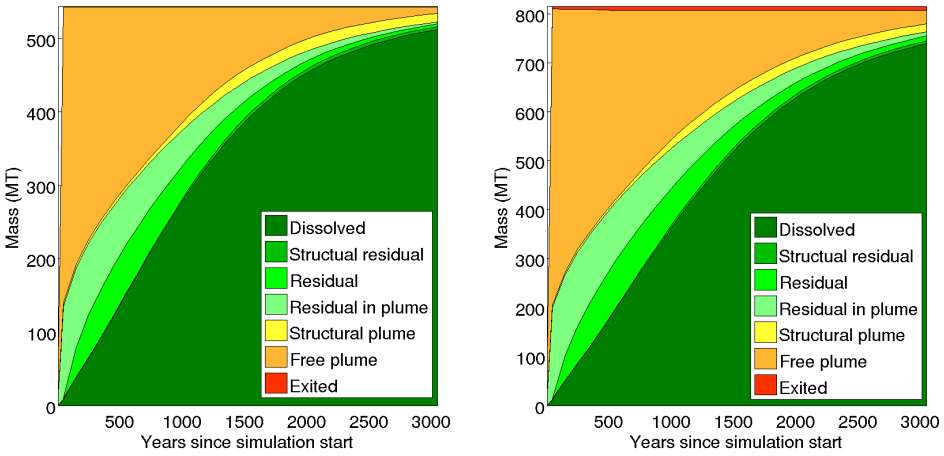


***Figure 8*** *Distribution of injected $CO_2$ in Scenario 1 as a function of time, including dissolution. Left diagram represents injection with the optimized schedule, and right diagram injection with 50% higher rates.*

After optimization of injection schedules, the total amount to be injected increases to 1598 Mt, an almost 80% increase. However, as can be seen on the resulting plume evolution plots on Figure 12, this increase is not evenly distributed among the injection sites. In particular, we note that the injection site in the middle region has been completely shut off. The reason is the leakage associated with injecting at this location. In the simulation involving *unoptimized* schedules, this site did manage to partly fill the small neighbor trap. However, during the injection process a significant amount of $CO_2$ was pushed the other way. This quantity quickly escaped up the steep slope towards the west during the migration period and left the aquifer domain. As the objective function used in the optimization process puts a large emphasis on preventing leakage ($W = 10$), the end result for this injection site was to be completely shut off. The right diagram of Figure 11 presents the distribution plot for this simulation. Out of 1.6 Gt of $CO_2$ injected, only 19 Mt, or 1.19%, has leaked. This is less than for the unoptimized case. However, we note that at 3050 years, around 20% of injected $CO_2$ is still freely flowing. If the simulation period had been further extended, parts of this quantity could still leak, forcing the optimization algorithm to reduce the injection rates. In other words, optimal use of the aquifer also depends on the time horizon considered.

*Scenario 3: Optimizing for an array of injection sites*

In the previous example, we noted that the optimization of injection schedules can cause some injection sites to become completely inactive. This observation leads to an alternative strategy for positioning injection sites. Instead of carefully selecting injection locations based on optimal use of structural traps, we can initially consider a large, evenly distributed array of injection sites that covers the whole domain of the aquifer. We then use the optimization of injection rates to identify sites that end up with zero or very small injection rates, and eliminate these sites. This approach treats all trapping mechanisms equally in the site selection process (although we have here excluded dissolution trapping, as explained above).

To test this approach at Utsira, we start with an initial, regular array of injection locations, measuring 99 km from east to west, 408 km from north to south, and consisting of 8 x 16 separate sites. We then remove all sites whose positions do not lie within the footprint of the aquifer, as well as all sites positioned over parts of the aquifer where $CO_2$ would be in a gaseous state. The location of the remaining sites can be seen as black dots in Figure 13. The initial, unoptimized schedule is defined by specifying a very large amount (4 Gt) to be injected over 50 years, evenly distributed across all sites. Although this amount is clearly in excess of what we expect to be able to store, we put the responsibility on the optimization algorithm to scale down rates where necessary to obtain an optimal set of schedules.

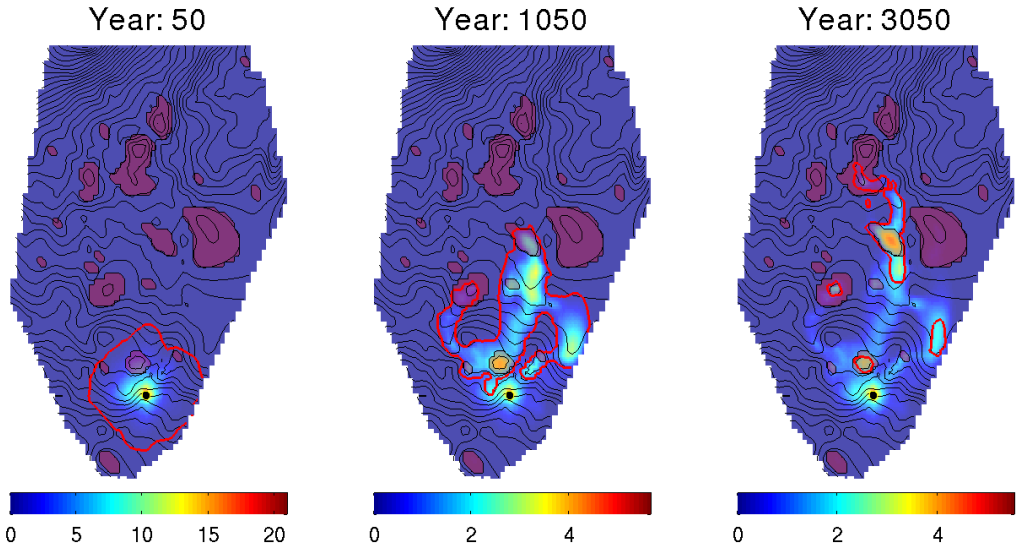


***Figure 9*** *Simulation of Scenario 1 with injection rate 50% higher than the optimized value, and with dissolution trapping included. $CO_2$ plume outlined in red, structural traps overlaid in purple. Total vertical integrated $CO_2$ content indicated with color (unit: tonnes per lateral square meter).*

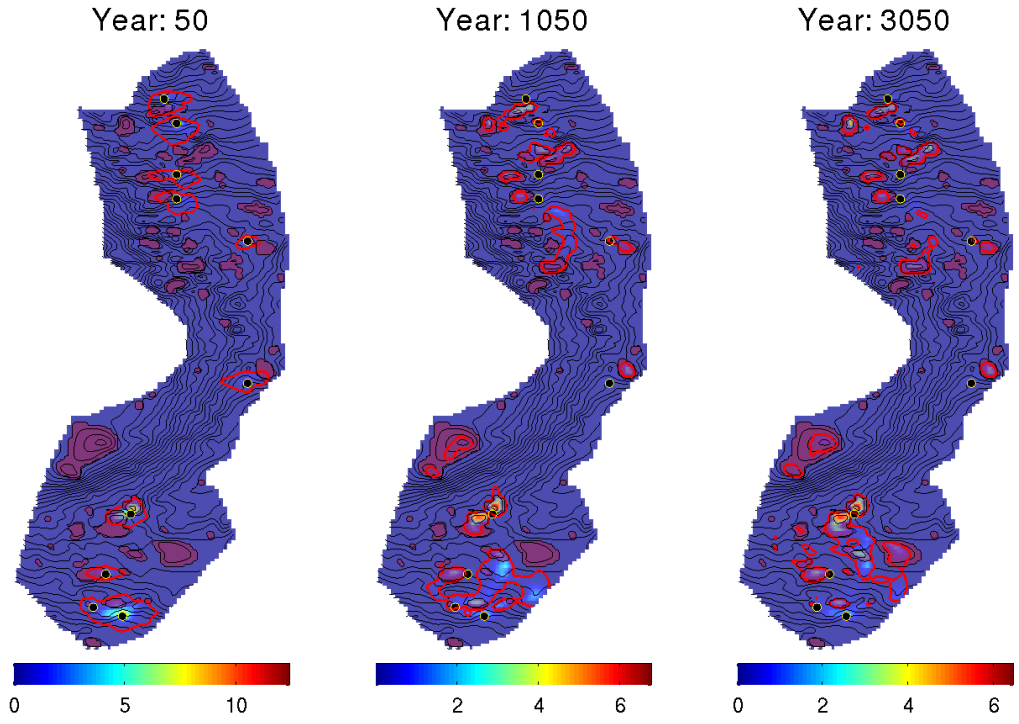


***Figure 10*** *Simulation of Scenario 2 with unoptimized injection rate. $CO_2$ plume outlined in red, structural traps overlaid in purple. Total vertical integrated $CO_2$ content indicated with color (unit: tonnes per lateral square meter).*

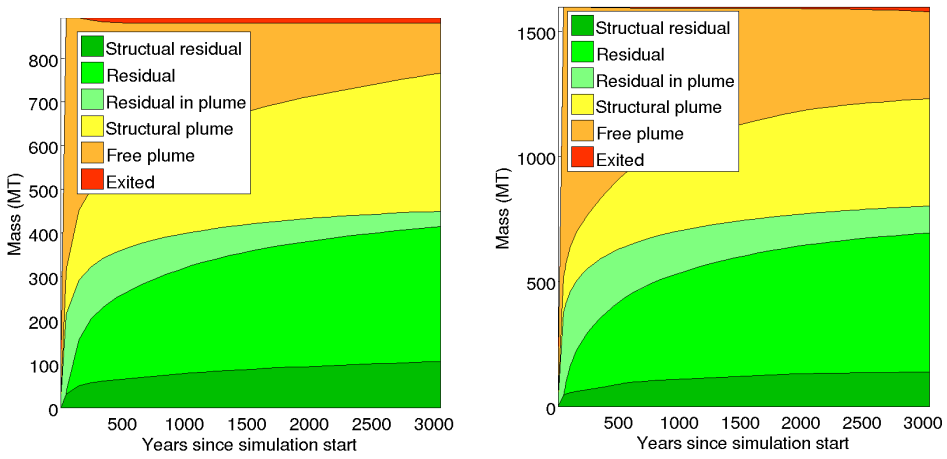


***Figure 11*** *Distribution of injected $CO_2$ in Scenario 2 as a function of time. Left diagram represents injection with unoptimized rates and right diagram with optimized rates.*

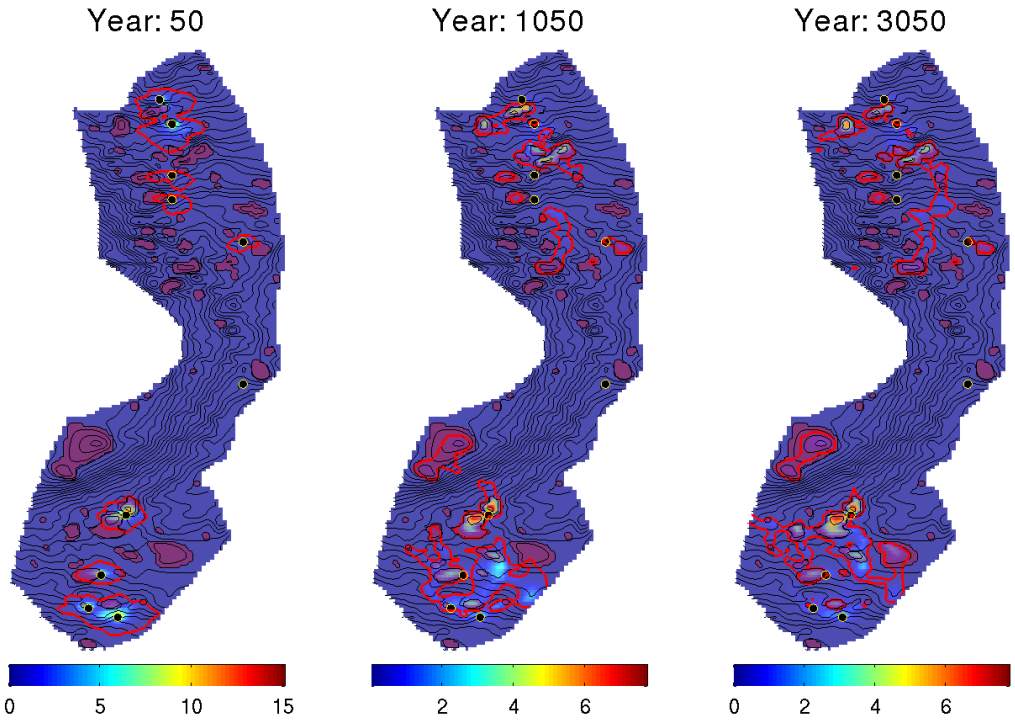


***Figure 12*** *Simulation of Scenario 2 after optimization of injection rate. $CO_2$ plume outlined in red, structural traps overlaid in purple. Total vertical integrated $CO_2$ content indicated with color (unit: tonnes per lateral square meter).*

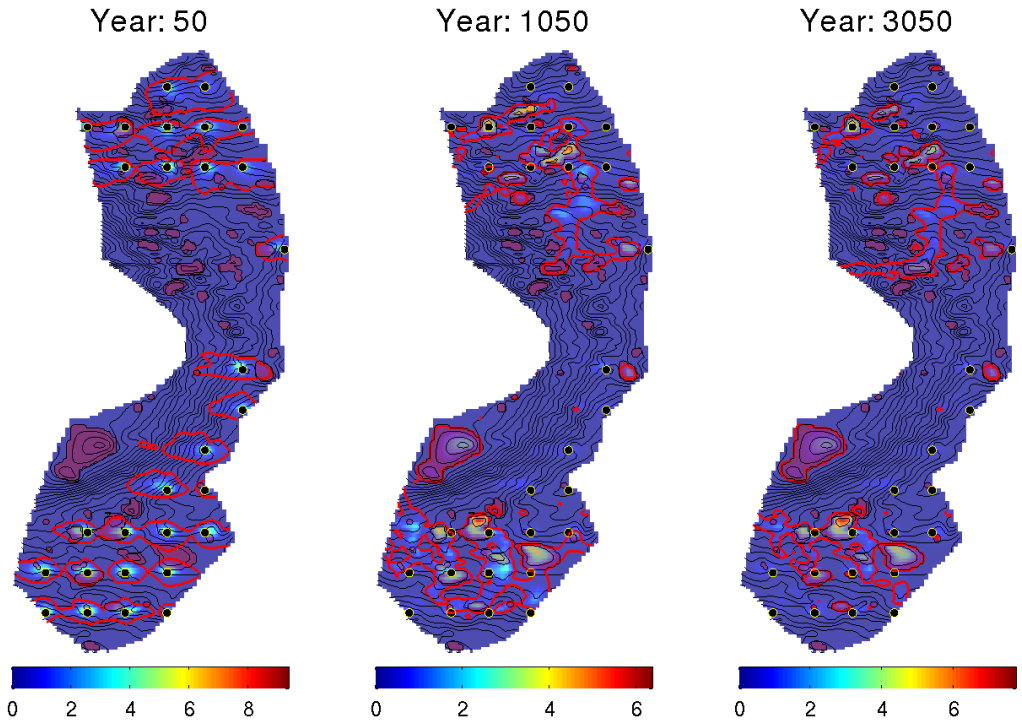


***Figure 13*** *Simulation of Scenario 3 with unoptimized injection rate. $CO_2$ plume outlined in red, structural traps overlaid in purple. Total vertical integrated $CO_2$ content indicated with color (unit: tonnes per lateral square meter).*

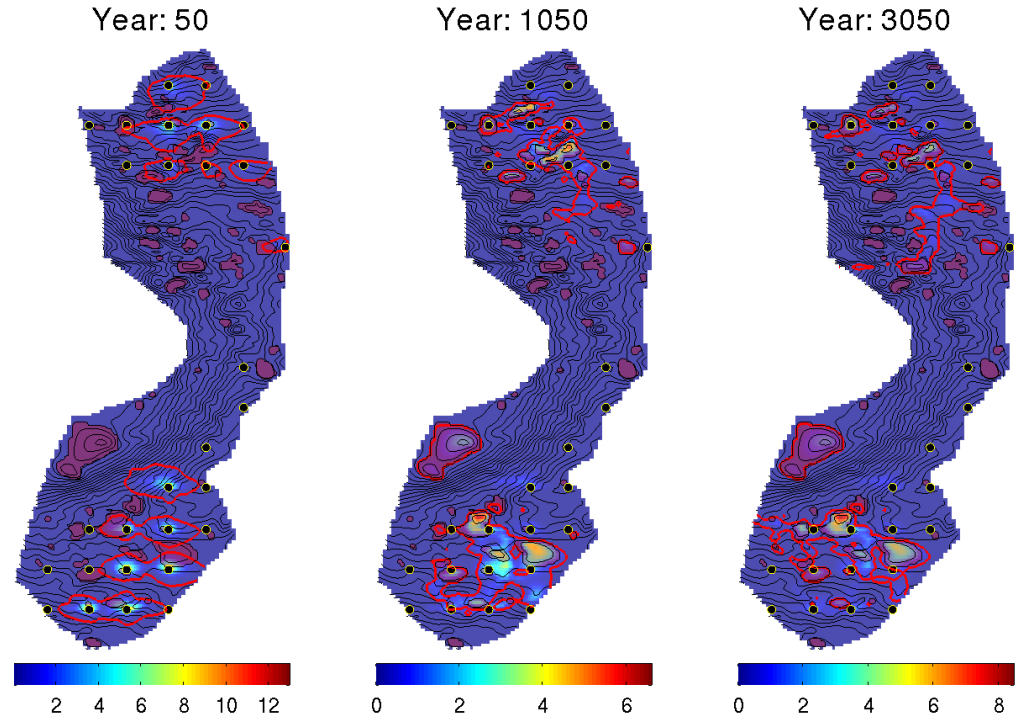


***Figure 14*** *Simulation of Scenario 3 after optimization of injection rate. $CO_2$ plume outlined in red, structural traps overlaid in purple. Total vertical integrated $CO_2$ content indicated with color (unit: tonnes per lateral square meter).*

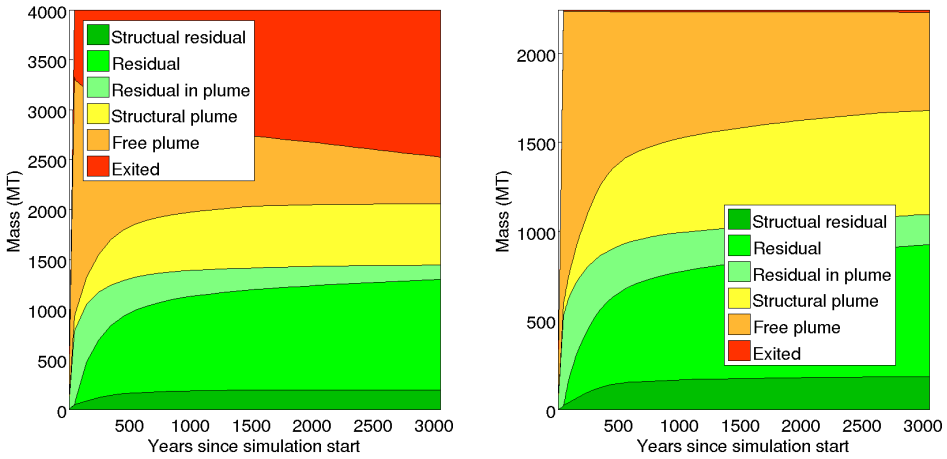


***Figure 15*** *Distribution of injected $CO_2$ in Scenario 3 as a function of time. Left diagram represents injection with unoptimized rates and right diagram with optimized rates.*

Running the simulation with the unoptimized schedules produces the results shown in Figure 13 and the left diagram of Figure 15. From the latter, we see that at the end of the injection period a large amount (almost 40%) of the injected $CO_2$ has leaked, as could be expected. Nevertheless, almost 2 Gt has been retained, predominantly as residual saturation. The large quantity of residually trapped $CO_2$ can be understood as a result of "flooding" the aquifer with large amounts of $CO_2$. Although much of it will leak back out, the size of the plume means that larger volumes of rock are reached, thus leaving behind more residually trapped $CO_2$. However, after approximately 1000 years the remaining free $CO_2$ primarily flows along previously visited pathways, and the amount of residually trapped $CO_2$ ceases to increase.

In Figure 14 and the right diagram of Figure 15, we see the result of simulating the scenarios with the optimized schedules. From the left plot of Figure 14 we note that only 14 of the initial 29 wells have actually injected $CO_2$, the rest being shut off. The shut-off sites include most of the sites along the eastern border, as well as some of the higher-lying sites in the northern and southern domains. Notably, no active injection site remains in the middle region. Using the optimized schedules, a total of 2.24 Gt is injected into the aquifer, with only 15.5 Mt (0.69%) escaped after 3000 years. From the distribution plot we see that while the total amount of realized structural capacity is approximately the same as in the unoptimized case, significantly less structural capacity has been realized. There is also a large quantity of free-flowing $CO_2$ remaining in the aquifer, so the potential for future leakage remains. Again, we see that optimal utilization of the aquifer will depend on the time horizon involved.

## Conclusion

Using available published information about the Utsira Formation, we estimate a maximal retaining capacity of 112 Gt of $CO_2$ for the aquifer. Of this, structural trapping constitutes 1.13 Gt, which lies wihtin the range of 0.5–1.5 Gt for the estimated prospectivity of the aquifer according to the Norwegian Petroleum Directorate. In addition, we estimate that the aquifer is capable of retaining 77 Gt of $CO_2$ by residual trapping and 34 Gt by dissolution into the remaining formation water. The combined estimate only provides a theoretical upper bound, as there is no practical way to achieve more than a small fraction of this capacity for a real scenario.

We have demonstrated two possible approaches for defining good injection scenarios, illustrated by a few simulated examples. In the most ambitious scenario tested, a total of more than 2.2 Gt of $CO_2$, injected from fourteen separate injection sites, was ultimately retained in the aquifer by structural and residual trapping alone, with only negligible volumes leaking across the boundaries of the aquifer model, during the 3000 year simulation period.

If the rate of $CO_2$ dissolution into brine at Utsira proves to be significant, the realisable storage potential of the aquifer could be significantly larger than we get from estimates neglecting this effect, as illustrated in our first scenario. However, at present, the role of dissolution for $CO_2$ storage at Utsira remains unclear. Another uncertain factor that can have significant impact on results is the exact division of the aquifer into regions where $CO_2$ is in gas and in dense phase. The boundary of this region is here only inferred based on the assumed temperature gradient and hydrostatic pressure. It should also be mentioned that the geometric analysis of the caprock that identifies traps and spill regions can be sensitive to small changes, so a thorough analysis should take resolution, precision, and level of noise in the input data into account. We would also like to underline that the lack of detailed petrophyical data is a signinficant cause of uncertainty. However, the methods we propose work equally well with heterogeneity and can be used to study this uncertainty if more data becomes available.

Finally, we emphasize that the amount of realizable trapping capacity in an open aquifer such as Utsira will highly depend on the time horizon considered as well as the total amount of leakage tolerated during the injection and migration processes.

## Acknowledgements

We thank Xavier Raynaud og Stein Krogstad for valuable contributions to the fully implicit solver and the adjoint calculations in MRST which we reused.

This work was founded by the MatMoRa-II project, Contract no. 21564 and Numerical $CO_2$ laboratory, Contract 199878 sponsored by the Research Council of Norway and Statoil ASA.

## References

Baklid, A., Korbøl, R. and Owren, G. [1996] Sleipner Vest CO2 disposal, CO2 injection into a shallow underground aquifer. *SPE Annual Technical Conference and Exhibition, 6-9 October, Denver, Colorado*, doi: 10.2118/36600-MS, sPE-36600-MS.

Chadwick, A., Arts, R., Bernstone, C., May, F., Thibeau, S. and Zweigel, P. [2008] *Best practice for the storage of CO2 in saline aquifers – Observations and guidelines from the SACS and CO2STORE projects*, vol. 14 of *British Geological Survey Occasional Publication*. British Geological Survey, Nottingham, UK.

Chadwick, R.A., Williams, G.A., Williams, J.D.O. and Noy, D.J. [2012] Measuring pressure performance of a large saline aquifer during industrial-scale co2 injection : the Utsira Sand, Norwegian North Sea. *Int. J. Greenh. Gas Control*, **10**, 374–388, doi:http://dx.doi.org/10.1016/j.ijggc.2012.06.022.

Gasda, S.E., Nordbotten, J.M. and Celia, M.A. [2011] Vertically-averaged approaches to CO2 injection with solubility trapping. *Water Resources Research*, **47**, W05528, doi:10.1029/2010WR009075.

Halland, E.K., Johansen, W.T. and Riis, F. (Eds.) [2011] *$CO_2$ Storage Atlas: Norwegian North Sea*. Norwegian Petroleum Directorate, P. O. Box 600, NO–4003 Stavanger, Norway.

Holloway, S., Chadwick, A., Lindeberg, E., Czernichowski-Lauriol, I. and Arts, R. [2004] Best practice manual from SACS–Saline aquifer CO2 storage project. Tech. rep., Statoil Research Center, Trondheim, Norway, IEA Greenhouse Gas R&D Programme, Schlumberger Research, European Commission.

Jansen, J.D. [2011] Adjoint-based optimization of multi-phase flow through porous media - a review. *Computers & Fluids*.

Lie, K.A., Krogstad, S., Ligaarden, I.S., Natvig, J.R., Nilsen, H.M. and Skaflestad, B. [2012] Open source MATLAB implementation of consistent discretisations on complex grids. *Comput. Geosci.*, **16**, 297–322, ISSN 1420-0597, doi:10.1007/s10596-011-9244-4.

Lie, K.A., Nilsen, H.M., Andersen, O. and Møyner, O. [2014] A simulation workflow for large-scale $CO_2$ storage in the Norwegian North Sea. *ECMOR XIV – 14$^{th}$ European Conference on the Mathematics of Oil Recovery, Catania, Sicily, Italy, 8-11 September 2014*, EAGE.

Lindeberg, E., Vuillaume, J.F. and Ghaderi, A. [2009] Determination of the CO2 storage capacity of the utsira formation. *Energy Procedia*, **1**(1), 2777–2784, doi:10.1016/j.egypro.2009.02.049.

MRST [2014] The MATLAB Reservoir Simulation Toolbox, version 2014a. `http://www.sintef.no/MRST/`.

Nilsen, H.M., Lie, K.A. and Andersen, O. [2014a] `MRST-co2lab`: sharp-interface models for fast estimation of trapping capacity. *submitted*.

Nilsen, H.M., Lie, K.A. and Andersen, O. [2014b] `MRST-co2lab`: vertical-equilibrium models with hysteresis and capillary fringe. *submitted*.

Nilsen, H.M., Lie, K.A., Møyner, O. and Andersen, O. [2014c] `MRST-co2lab`: spill-point analysis and structural

trapping capacity in saline aquifers. *submitted*.

Nordbotten, J.M. and Celia, M.A. [2012] *Geological Storage of CO2: Modeling Approaches for Large-Scale Simulation*. John Wiley & Sons, Hoboken, New Jersey.

Raynaud, X., Krogstad, S. and Nilsen, H.M. [2014] Reservoir management optimization using calibrated transmissibility upscaling. *ECMOR XIV – 14th European Conference on the Mathematics of Oil Recovery, Catania, Sicily, Italy, 8-11 September 2014*, EAGE.

Singh, V., Cavanagh, A., Hansen, H., Nazarian, B., Iding, M. and Ringrose, P. [2010] Reservoir modeling of $CO_2$ plume behavior calibrated against monitoring data from Sleipner, Norway. *SPE Annual Technical Conference and Exhibition, 19-22 September 2010, Florence, Italy*, doi:10.2118/134891-MS, sPE 134891-MS.

Span, R. and Wagner, W. [1996] A new equation of state for carbon dioxide covering the fluid region from triple-point temperature to 1100 K at pressures up to 800 MPa. *J. Phys. Chem. Ref. Data*, **25**(6), 1509–1597.

Thibeau, S. and Mucha, V. [2011] Have we overestimated saline aquifer CO2 storage capacities? *Oil Gas Sci. Technol. – Rev. IFP Energies nouvelles*, **66**(1), 81–92, doi:10.2516/ogst/2011004.

UNFCCC [2011] `http://unfccc.int/di/FlexibleQueries.do`, query parameters: Europe27, 2011, net emissions excluding land use, CO2 only, total for categories 1.A.1 (Energy Industries) and 1.A.2 (Manufacturing Industries and Construction).